Design of a 1000 N N2O/Paraffin-ABS Hybrid Rocket Engine for a Reusable VTVL Lander

Sukhmani Sethi*, Matthew Xu*, Veer Gudkha*, Felix Gusic*, Chengle Qian†, Val Donchev‡, Amaan Patel†, Grace Dilgard*, Michael Swoyer*, Chen Szu Heng*

The development of reusable rocket technology at the collegiate scale requires a propulsion architecture that prioritizes both safety and technical feasibility. Hybrid rocket engines offer a compelling framework for vertical takeoff, vertical landing (VTVL) applications due to their ease of development, inherent safety, and throttleability. To explore these capabilities at the student scale, a VTVL lander is under development by Propulsive Landers at Georgia Tech with a mission profile consisting of a 10 s tethered hover test, a 10 m vertical descent and landing maneuver, and a 50 m vertical hop with controlled landing. This paper details the design of a 1000 N N2O/Paraffin-ABS hybrid rocket engine intended as the primary propulsion system for the lander. Engine design was driven by thrust and safety requirements while supporting a reusable architecture for rapid development. Component dimensions for the fuel grain, injector, and pre/post combustion chamber were optimized using first-order approximations and parameters from existing literature. The work documents the full development process of the engine up to an initial hotfire and outlines lessons learned and a path forward for continued improvement.

I. Introduction

Vertical Take-off, Vertical Landing (VTVL) architectures are essential to the development of reusable rocket technologies. For VTVL platforms to achieve their purpose, they must execute powered descent which naturally imposes stringent propulsion requirements including deep throttle and restart capability. Meeting these requirements is contingent on the underlying propulsion architecture. Among the available options, liquid bi-propellant systems have traditionally been the preferred choice for propulsive landing due to their high specific impulse and higher throttle response [1]. However, these performance advantages come at the cost of increased system complexity with liquid rocket engines requiring dual propellant feed systems that increases the amount of hardware and plumbing required [2]. In many implementations, liquid systems also rely on cryogenic propellants that bring additional burdens and introduce requirements such as insulation and cooling during fill procedures. [3] Additionally, solid rockets are incompatible with VTVL requirements because the propellant is a singular solid grain and lacks restart capabilities. Since the burn rate is restricted by a fixed grain geometry, the system cannot provide the dynamic thrust control necessary for vertical landing. [4]

Hybrid rocket engines present a compelling alternative that addresses many of these constraints [5]. Their inherent physical separation of oxidizer and solid fuel provides a significant safety margin, and throttleability via oxidizer mass flow modulation through a single feed line reduces system complexity relative to liquid bipropellants [6]. The solid fuel grain can also be tailored in both composition and geometry to meet specific performance and manufacturability requirements, a flexibility that is particularly relevant under the fabrication constraints and rapid iteration demands of a student team. [7] Novel fuel formulations combining liquefying fuels with structural reinforcement strategies have demonstrated potential to address longstanding limitations of hybrid engines such as low regression rate and mechanical fragility [8, 9]. Despite these advantages, hybrid VTVL systems at the collegiate scale remain largely undocumented in formal literature, representing an open area for development and validation.

This work presents the design, modeling, manufacturing, and validation of a 1000 N class hybrid rocket engine developed by Propulsive Landers at Georgia Tech (GTPL) as the primary propulsion system for its reusable VTVL lander program. The lander mission profile consists of a 10 s tethered hover test, a 10 m vertical descent and landing maneuver, and a 50 m vertical hop with controlled landing, driving the propulsion requirements that shaped the engine design presented in this work.

*Undergraduate Student, Guggenheim School of Aerospace Engineering, Atlanta, GA, 30332, AIAA University Student.
†Undergraduate Student, Woodruff School of Mechanical Engineering, Atlanta, GA, 30332, AIAA University Student.
‡Masters Student, Guggenheim School of Aerospace Engineering, Atlanta, GA, 30332, AIAA University Student.

II. Engine Design Choices

A. Propellant Selection

Liquid nitrous oxide and paraffin-ABS were selected as the oxidizer and fuel combination. Nitrous oxide was chosen primarily for its high liquid density and storability at ambient temperature. Although N2O is often known for its self-pressurizing properties, an externally-pressurized sub-cooled N2O was ultimately chosen to avoid having to model the full-physics of blowdown during flight. In a blowdown configuration, pressure decreases continuously as oxidizer mass is depleted and the internal thermodynamic state of the tank evolves according to saturation equilibrium. As the ullage volume expands and tank temperature decreases, the system also transitions through nonlinear two-phase dynamics that are coupled to feed pressure and oxidizer mass flow rate which are difficult to model in real-time [10]. Sub-cooled liquid delivery therefore provides a more predictable and controllable oxidizer supply, which is critical for a throttleable VTVL application.

Paraffin wax was chosen as the primary fuel of the engine. Unlike conventional hybrid fuels such as HTPB, PMMA, and HDPE that undergo a turbulent boundary layer combustion mechanism, paraffin wax's primary mass transfer mechanism occurs through droplet entrainment which is less susceptible to the blowdown effect that limits the fuel's regression rate [10–12]. Consequently, this allows the engine to satisfy a lower L/D ratio and reduce mass budget pertinent to the structural components of the lander [13]. However, paraffin exhibits relatively poor mechanical strength and is therefore prone to cracking under thermal and mechanical loading during combustion [**?**] To address these limitations, the fuel grain incorporates a 3D-printed ABS-gyroid structure that serves the two purposes of (1) increasing mechanical strength of the fuel grain (2) and manufacturability. [6, 14]. Gyroids are a triple periodic minimal surface geometry that provides near isotropic behavior when compared to a conventional lattice. The geometry allows the distribution of stresses evenly and theoretically mitigates the crack propagation along a single axis [8, 15]. Beyond aspects related to structural reinforcement, the gyroid also plays an important role in manufacturability especially under the demands of frequent engine hotfires. Instead of complex multi-part molds or post-cure reinforcement processes typically seen in pure paraffin grains, here the grain can be casted directly into the printed structure under the right temperature conditions [8, 16].

B. Chamber Pressure Selection

A nominal chamber pressure of 40 bar was selected based on a combination of oxidizer property constraints and system-level pressure drop considerations. In general, higher chamber pressure is desirable as it improves characteristic velocity and specific impulse [1]. For paraffin specifically, higher chamber pressure also enhances droplet entrainment by increasing gas-phase density and interfacial shear at the melt layer, driving higher regression rates [11]. However, the practical upper bound on chamber pressure is constrained by the available upstream supply pressure of the oxidizer.

Nitrous oxide stored as a saturated liquid at ambient conditions exhibits a saturation pressure of approximately 52–55 bar at typical storage temperatures [17]. To ensure single-phase liquid delivery and provide sufficient margin above the saturation pressure, an upstream tank pressure of 65 bar was selected via external pressurization. This 65 bar supply pressure must then account for losses across the feed system components and the required pressure drop across the injector. With a target injector stiffness ratio of 20%, the injector itself consumes 8 bar of the available pressure budget at the nominal 40 bar chamber pressure. The remaining margin accommodates losses across valves, fittings, and feed line segments. A chamber pressure of 40 bar therefore represents a value that satisfies the injector stiffness requirement while remaining comfortably within the pressure budget imposed by the 65 bar supply, and is consistent with operating pressures reported in comparable 1 kN-class paraffin hybrid engines in literature [18, 19].

III. Engine Sizing Methodology

A. Governing Internal Ballistics Model

The engine was designed to deliver a target thrust of 1000N at the nominal chamber pressure of 40 bar. These requirements were derived from the minimum lander thrust-to-weight ratio of 1.2 imposed by the GTPL VTVL flight envelope. A single circular-port grain geometry was adopted over configurations such as multi-port designs given its simplicity [18]. For sizing purposes, oxidizer mass flow rate $\dot{m}_{ox}$ and fuel grain length L were treated as the primary design variables. To begin modeling the grain evolution and overall engine behavior, it is first necessary to describe the regression process that governs the fuel mass flow rate of the engine. Regression rate, most importantly, can be defined as the rate at which the radius of the port expands over time. For both liquefying (paraffin wax, beeswax) and non-liquefying fuels (HTPB, PMMA, HDPE), the regression rate follows a power-law dependence on oxidizer mass flux and commonly expressed as [11, 14]:

$$\dot{r} = aG_{ox}^{n} \tag{1}$$

where the oxidizer mass flux is defined as

$$G_{ox} = \frac{\dot{m}ox}{Aport}. \tag{2}$$

This flux represents the amount of oxidizer passing through the fuel grain per unit area, directly influencing the heat transfer to the fuel surface [11]. For a circular port, the cross-sectional area changes over time as fuel is consumed:

$$A_{port}(t) = \frac{\pi}{4} D_p(t)^2. \tag{3}$$

The instantaneous fuel mass flow rate is then determined by the fuel density ρ_f, the length of the grain L, and the ever-changing burning surface area:

$$\dot{m}_f(t) = \rho_f \pi D_p(t) L \dot{r}(t), \tag{4}$$

and total mass flow rate is the sum of the solid fuel pyrolysis products and the gaseous oxidizer:

$$\dot{m}t(t) = \dot{m}ox + \dot{m}_f(t). \tag{5}$$

Assuming quasi-steady choked flow at the throat, the chamber pressure is derived from the total mass flow and the characteristic velocity C^*, which accounts for the combustion efficiency of the propellant combination:

$$P_c(t) = \frac{\dot{m}_t(t) C^*}{A_t}, \tag{6}$$

and thrust is computed using the thrust coefficient C_F, which is a function of the nozzle expansion and ambient pressure:

$$T(t) = C_F P_c(t) A_t. \tag{7}$$

Finally, the port diameter evolution follows a rate of change equal to twice the regression rate, as the fuel recedes radially from the centerline:

$$\frac{dD_p}{dt} = 2\dot{r}. \tag{8}$$

B. Numerical Implementation

After a full derivation, the full internal (simplistic) ballistic problem is now fully defined. With the relationship established, the sizing task becomes one of selecting the correct mass oxidizer flow rate and grain length such that the time-averaged thrust satisfies the 1000N requirement while the average oxidizer-to-fuel ratio remains within an acceptable range by the tradeoffs of chamber temperature, Isp, and characteristic velocity [1]. As reflected in the equations above, since thrust and mixture ratio are both nonlinear functions of various engine parameters (all of which are time variant), the problem cannot be reduced to solving a single closed-form algebraic equation. Instead, the governing equations form a coupled, time-dependent system which therefore necessitate a numerical approach capable of modeling the internal ballistic evolution over burn duration until convergence is achieved by both criteria of thrust and mixture ratio [14]. For those purposes, the equations above were translated into a custom numerical solver. The model inputs used for all sizing calculations are summarized in Table 1.

Table 1 Hybrid engine numerical model inputs.

Parameter	Value	Units
Target average thrust	1000	N
Target average O/F	7.1	–
Initial port diameter $D_{p,i}$	0.05	m
Regression coefficient a	9.00×10^{-5}	m/s

Table 1 (continued): Hybrid engine numerical model inputs.

Parameter	Value	Units
Regression exponent n	0.67	–
Fuel density ρ_f	900	kg/m^3
Chamber pressure P_c	40	bar
Characteristic velocity C^*	1151	m/s
Specific Impulse I_{sp}	215	s
Thrust coefficient C_F	1.5025	–
Combustion efficiency η_c	0.90	–
Nozzle efficiency η_n	0.90	–
Combined Efficiency η	0.81	–

Using the parameters in Table 1, the solver then evaluates the instantaneous port diameter from the integrated regression relation. At each time step, the oxidizer mass flux is calculated from the evolving port area and regression rate is continuously evaluated using the power-law. The instantaneous fuel mass flow rate is then determined then used to calculate the thrust using the total mass flow rate, characteristic velocity, and efficiency factors including η_c, η_n. Upon convergence, the solver outputs: required fuel grain length, required oxidizer mass flow rate, time-averaged thrust, time-averaged mixture ratio, throat area and diameter, and exit area and diameter. These results are used to define the baseline engine geometry presented in the following section.

C. Engine Design

The converged geometric parameters obtained from the solver then defines the engine that was later manufactured by Georgia Tech's Montgomery Machining Mall. The engine was designed as a modular assembly consisting of a pre-combustion chamber, showerhead injector plate, fuel grain, and a nozzle. The combustion chamber and injector were manufactured from aluminum 6061 for a balance of mass and strength. Wall thickness were selected with a safety factor of 2.5 and FEA was conducted to analyze Von Mises stress and review for potential failure modes. The final engine is shown in Figure 1.

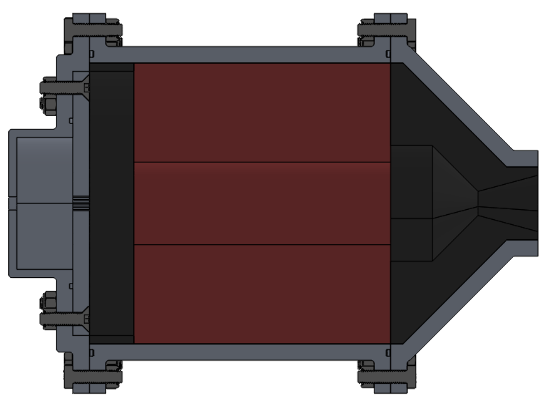

Fig. 1 Engine Cross-Section

In this engine, a showerhead injector was chosen for its geometric simplicity and manufacturability. Although alternative injector configurations such as swirling injectors have the ability to increase regression rate locally by means of higher tangential momentum and improved oxidizer mixing, they lead to uneven regression axially across the grain, which is undesirable over extended burn durations, especially for paraffin wax [19–21]. Showerhead injectors, by contrast, promote a more uniform axial distribution into the port [19] and can still be designed and optimized with ease by means of SMD correlations. In this design, the showerhead injector plate consists of 114 equally spaced orifices with an injector stiffness ratio of 20%. Using a discharge coefficient of 0.32 (to account for the effects of flashing) [1, 22] and a density of $750\,\mathrm{kg\,m^{-3}}$, the required injector area was calculated to be $5.41 \times 10^{-5}\,\mathrm{m^2}$. Dividing this area across 114 orifices gives a single-orifice diameter of 0.78 mm. The injector was designed with a target SMD of approximately 1900 µm.

D. Fuel Grain Manufacturing

The fuel grain was manufactured to match the dimensions in provided in the outputs of the script. This section covers the fabrication process developed to minimize casting defects whilst maintaining structural integrity. Because paraffin wax exhibits relatively low tensile strength and is susceptible to crack formation during both cooling and combustion, additional structural reinforcement was required. A 3D-printed ABS gyroid structure was fabricated to act as an internal skeleton. The structure was created via the use of Cura Ultimaker where the infill pattern was set to a gyroid geometry with a fill percentage of 15%. The decision was based on the literature by Bisin and Paravan in which a 15% infill percentage provided ample structural stability while having minimal impact on fuel regression rates [8].

In the casting process, a cleaned stainless steel pot was filled with solid paraffin pellets and heated gradually to approximately 125°C in order to completely melt the paraffin crystalline structure [23]. During melting, paraffin was stirred continuously to promote uniform temperature distribution and prevent localized hot spots. Once target temperature was achieved, the heat source was removed and the paraffin was allowed to cool to approximately 80-90°C before it is poured into the ABS. The selected temperature for paraffin wax was chosen to remain below the glass transition temperature of ABS, avoiding case deformation. Prior to casting, the ABS mold was wrapped in aluminum foil and placed on a cooling plate maintained near 0°C to induce a 1-D thermal gradient within the grain.

One dimensional cooling is an integral mechanism in ensuring the quality of fuel grains. Insulating material is wrapped around the casing to ensure minimal heat exchange with ambient air. Non-homogeneous thermal gradients occur when heat exchange occurs predominantly laterally between grain walls and ambient air. Such gradients are more likely to cause void deformations due to the disparity of paraffin's density between solid and liquid states combined with uneven cooling patterns[16].

The paraffin was then poured into the mold in a controlled, multi-layered process. In the procedures, each layer was given the time to partially solidify before the next layer was added. This gives the paraffin time to shrink gradually and for the entire mold to be filled. After the final layer was poured, the grain was left undisturbed to cool completely to room temperature. Once solidified, the grain is visually inspected before it is inserted into the engine. A post-inspection of the fuel grain is included in the result section of the paper.

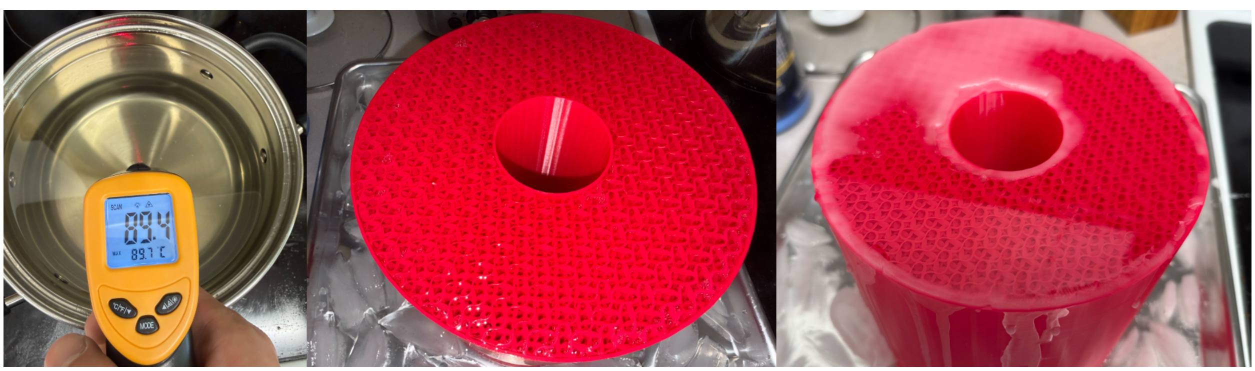

Fig. 2 Grain Manufacturing Process

IV. Propellant Feed System

The role of the Propellant Feed System (PFS) is to regulate the delivery of oxidizer from the source tank into the engine. For the engine, the PFS was designed to meet a target mass flow rate of 0.561 kg/s and a chamber pressure of 40 bar. The physical layout of this design is presented in the Piping and Instrumentation Diagram (P&ID) shown in Fig. 3 which maps the specific arrangement of valves, sensors, and feed lines on the system.

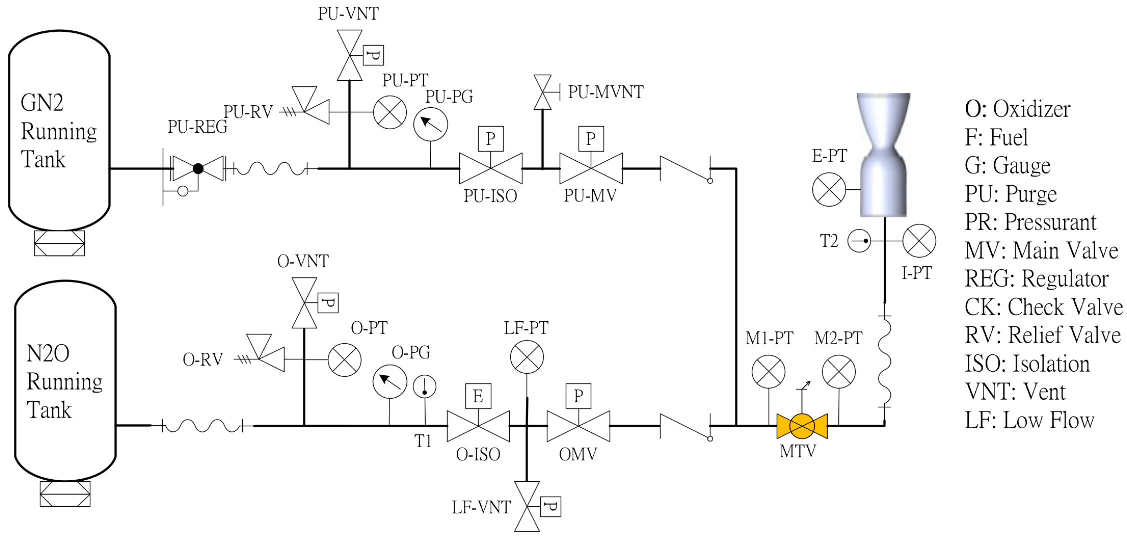

Fig. 3 P&ID of Test Stand

A. Propellant Feed System Pressure Loss Modeling

The pressure drop calculations across the propellant feed system were computed component-by-component and assembled into a pressure ladder of descending pressure from the oxidizer tank to the combustion chamber. The component-wise pressure drops were calculated using two different methods. The Darcy-Weisbach equation was used to calculate the pressure drop across the piping segments:[24]

$$\Delta P = f \cdot \frac{L}{D} \cdot \frac{\rho v^2}{2} \tag{9}$$

This model factors in the constant energy loss from velocity changes and boundary layer formation near the pipe walls. In longer sections, the buildup of wall friction causes a significant drop in overall pressure. In contrast, local pressure drops across valves, filters, elbows, and fittings were calculated using the minor loss equation:[25]

$$\Delta P = K \cdot \frac{\rho v^2}{2} \tag{10}$$

These losses are independent of pipe length because they are caused by localized geometry changes rather than wall friction [17]. Finally, the system pressure was controlled using the regulators shown in the P&ID to ensure the flow reached the combustion chamber at the target pressure.

B. Flow Control and Throttling

The feed system uses a Main Throttle Valve (MTV) as the primary thrust control mechanism to regulate the oxidizer mass flow rate by modulating the effective flow area. The MTV provides control over instantaneous thrust by changing mass flow rate. As the valve opens, the ball rotates to a specified angle, directly adjusting the flow area and therefore the mass flow rate through the oxidizer line. The low flow branch was a temporary solution for managing ignition transients prior to the MTV being manufactured; however, the MTV is capable of handling both ignition transients and full throttling across the entire range of operation. Integrating the MTV eliminates the need for a secondary ignition line while providing greater throttling capability. [6, 26].

C. Safety Systems and Components

Numerous safety measures are implemented throughout the propellant feed system. Check valves are used to protect against backflow in the event of dangerous downstream conditions. During ignition, combustion, or combustion instability, chamber pressure could exceed upstream pressure. Check valves ensure flow moves in only one direction, physically preventing reverse flow from reaching upstream components such as regulators, sensors, or the running tank.

Another key safety component is the oxidizer isolation valve (O-ISO) which was determined to be electric because it enables redundant control of the main oxidizer line with a different approach in case pneumatics fail. Since the oxidizer line carries N_2O, having an independent electrical actuation pathway ensures the system retains the ability to cut off oxidizer flow even under a complete loss of pneumatic pressure.

To prevent unintentional entry into the system, valves along the flow path are set to be closed in their default state. The valves used to vent the system are set to open as their default state to ensure that there are no trapped volumes within the system. In case of emergencies, default states prevent more oxidizer from entering the engine and allow the system to depressurize through the vents. The purge line serves a distinct safety function within the feed system. While the oxidizer line delivers N_2O to the engine during a test, the purge line — pressurized with GN_2 and controlled through PU-ISO and PU-MV — is designed to clear the system of residual oxidizer before and after operation. Introducing an inert gas into the lines displaces any remaining N_2O, eliminating the risk of oxidizer accumulating or being present when the system is approached by personnel.

Table 2 Normal States of Feed System Components

Abbr.	Full Name	State	Abbr.	Full Name	State
O-VNT	Oxidizer Vent	Normally Open	PU-VNT	Purge Vent	Normally Open
O-ISO	Oxidizer Isolation	Normally Closed	PU-ISO	Purge Isolation	Normally Closed
LF-VNT	Low Flow Vent	Normally Open	PU-MVNT	Purge Manual Vent	N/A
OMV	Oxidizer Main Valve	Normally Closed	PU-MV	Purge Main Valve	Normally Closed
MTV	Main Throttle Valve	Normally Closed			

D. Discharge Coefficient Characterization

Cold-flow testing was conducted to validate the theoretical pressure ladder against empirical data. The mass flow rate was derived from a tank weight differential over a 3-second duration to establish a baseline for the system discharge coefficient. The experimental $C_d A$ was determined using the calculated mass flow and average upstream pressure recorded during the blow-down transient as shown in Fig. 4:

$$C_d A = \frac{\dot{m}}{\sqrt{2\rho\Delta P}} \tag{11}$$

A mass differential of 1.46 kg was observed across the tanks, which yielded an oxidizer mass flow rate of 0.487 kg/s. Cold flow testing was conducted at an ambient temperature of 49°F. Based on NIST reference tables, the density of nitrous oxide was determined to be 856.07 kg/m^3. The upstream pressure had an initial pressure of 42.662 bar and a final pressure of 40.88 bar upon MTV closure. By taking the average of these pressures and accounting for an ambient pressure of 1.013 bar, the pressure drop was found. Using Equation (9), the resulting discharge coefficient area ($C_d A$) was calculated as 5.83×10^{-6} m^2.

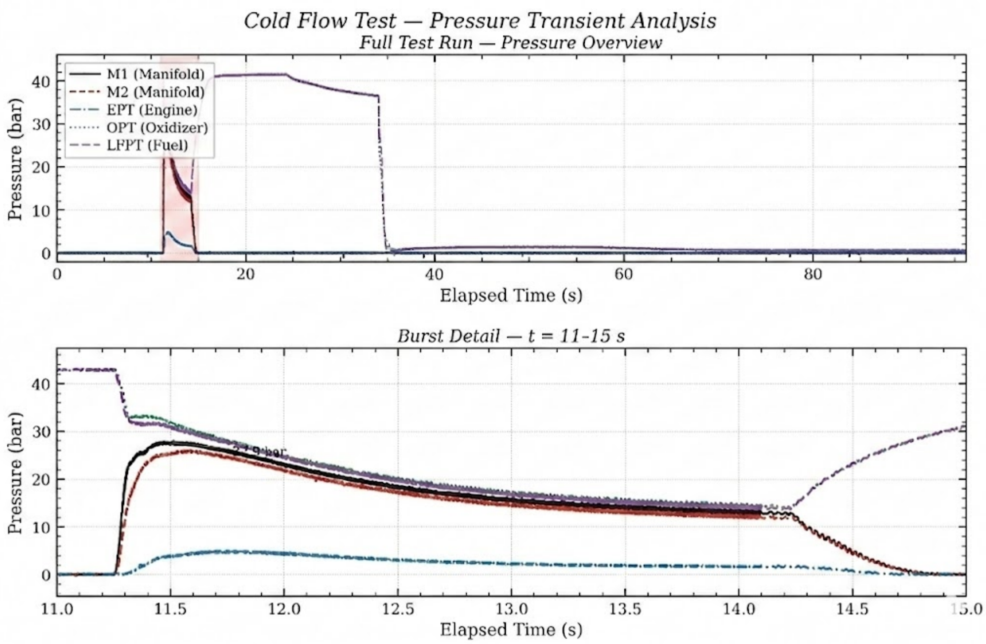

Fig. 4 Cold Flow Data

V. Results and Discussion

At the time of writing, five cold-flow tests and two hot-fire tests have been conducted. As a result of DAQ malfunctions during both hot-fire attempts, pressure and thrust were not successfully recorded. As a result, this section presents only qualitative observations and post-fire inspection. Despite issues with data collection, the team successfully demonstrated a nitrous ignition and a sustained flame was observed. The resulting hotfire is shown in Figure 5

Fig. 5 Snapshot of Engine Hotfire

Post-fire inspection of the fuel grain revealed a relatively steady conical regression profile originating near the injector face. A cylindrical regression pattern is observed extending 22.35 mm from the injector side down the port axis, followed by the conical regime. The injector facing side of the fuel grain experienced greater regression compared to the aft region with a final port diameter. A final port diameter of 53.98 mm on the nozzle end, 68.01 mm on the injector end, and 87.63 mm for the cylindrical regime were observed from a uniform starting diameter of 50 mm. Regression walls along the conical regime are smooth, suggesting a steady regression pattern. Uneven wall smoothness suggest more unstable regression behaviors in the conical section. The axial variation is consistent with higher oxidizer mass flux near the injector entrance and gradual reduction in mass flux as the flow develops downstream [11, 13, 27]. From a starting mass of 2.94 kg, a mass of 2.4 kg was observed following hot-fire, totaling 0.59 kg of propellant used during a 5 second burn.

Additionally, the measured $C_d A$ was significantly lower than the values predicted by the pressure ladder. This discrepancy is likely due to nitrous oxide's two-phase flow. As the static pressure dropped across internal orifices, conditions likely fell below the oxidizer's vapor pressure, which induces flashing. This phase change results in choked flow conditions, where the formation of gas increases the specific volume of fluid at the orifice, restricting the mass flow rate regardless of the upstream pressure [10, 17].

VI. Challenges

Throughout the manufacturing process of the engine to until the hotfire, the team faced several challenges that will be addressed in the following section. The intention of this discussion is not only to document specific obstacles but also shed light on realities faced by student teams practicing rocketry at the collegiate level.

A. Data Acquisition System and Valve Actuation

One of the most significant challenges encountered during testing was related to the setup and data collection of our DAQ device. The DAQ used by Propulsive Landers is responsible for both acquiring sensor inputs and issuing the commands which actuate the valves. In addition to recording all pressure values across the feed system and load cell data, it also works directly with the solenoid valves to control the flow of our oxidizer and nitrogen purge. Across multitude of tests, a substantial portion of the test time was allocated to diagnosing DAQ-related issues which drastically hindered our test timeline. The current DAQ also fails to collect and record data at the frequency it is needed.

B. Learning-By-Doing Philosophy

As a collegiate rocketry team, much of the development within the team occurs within a learning-by-doing framework. Unlike established organizations with long-standing institutional knowledge and persons of expertise, knowledge is accumulated slowly through design reviews, manufacturing attempts, test failures, and subsequent refinements. Engineering insights are often not realized during early stages of the project but only after the hardware has been assembled. In practice, this means that understanding is often built from the ground up and as such members eventually learn not only how subsystems work and when their assumptions fail. However, this also means that progress is never linear and time must often be allocated revisiting assumptions and re-evaluating design choices that previously were sound. Though rewarding, this dynamic can become challenging when the team is simultaneously pushing toward ambitious milestones and scheduled test campaigns. The pressure to demonstrate measurable progress must often be balanced against the need to slow down, reassess, and strengthen foundational understanding. Although such experiences are rarely detailed in proceeds as such, they form a significant part of collegiate rocketry team culture and a merit discussion.

C. Knowledge Transfer

Another persistent challenge is the knowledge transfer across academic cycles. Student teams such as Propulsive Landers at Georgia Tech experience continual membership turnover, as experienced members graduate or transition to internships while new members join and begin developing technical familiarity with the project. This means that throughout an entire project's life cycle there must be intentional effort in maintaining documentation. While this may appear straightforward in principle, in practice it is difficult to execute especially when teams are operating under serious time constraints.

VII. Conclusion and Future Work

This paper documented the design, manufacturing, and preliminary testing of 1000 N N_2O/Paraffin-ABS hybrid rocket engine intended for the GTPL reusable VTVL lander. A numerical internal ballistics model was developed to size the fuel grain, injector, and combustion chamber geometry to meet the lander's thrust and mixture ratio requirements. The N_2O/Paraffin-ABS propellant combination was selected to satisfy the throttleability and storability demands of the VTVL mission, while the gyroid grain structure addressed the mechanical limitations of pure paraffin fuels. Cold-flow testing yielded a mass flow rate and $C_d A$ below predicted values, likely due to two-phase flashing at internal orifices driving choked flow conditions and restricting oxidizer delivery. Although DAQ failures prevented quantitative performance validation during hotfire, sustained combustion was demonstrated and post-fire grain inspection revealed regression behavior consistent with model predictions. The work establishes a design baseline and manufacturing process for continued development toward the full GTPL mission profile.

Future iterations of the HRE will focus on refining the feed system to maintain a single-phase liquid delivery and improve the system reliability. To mitigate the flashing and subsequent choked flow observed during the cold flow testing, the system's operating conditions will be modified. Specifically, an increase in both the upstream tank pressure and the nominal chamber pressure will be implemented to ensure the oxidizer remains significantly above its vapor pressure. This change is intended to minimize pressure drop and stifle the formation of a gas phase at internal orifices, preventing the mass flow from being restricted and allowing the system to reach the target 0.561 kg/s prior to future hotfire and testing.

Testing plans for the current 1000N engine revolve around its future integration onto a working lander. Subsequent testing will include elevated pressure cold-flow runs to confirm single-phase oxidizer delivery at the 0.561 kg/s target, followed by a hotfire campaign to validate the 1000 N thrust prediction and characterize MTV throttle response across its full operating range. Upon engine validation, the system will be integrated onto the lander toward the full GTPL mission profile.

Future combustion chamber tests involve improving the stability and repeatability of combustion mechanics. Two separate igniter systems will be developed successively for subsequent stages of testing. A pyrogen igniter is being developed to improve the reliability of engine starting characteristics for near future tests. For applications involving restart capability, a torch igniter is being developed, allowing the lander to hop to a specified location and restart ignition at each location. The pyrogen igniter will help to pinpoint exact conditions required to start a sustainable chain reaction. This data will then be used as performance parameters in subsequent torch igniter development, ensuring reliable start performance.

Nozzle thermal management represents another critical area for future development. Preliminary thermal analysis of the current aluminum nozzle revealed that convective heat flux peaks sharply at the throat, reaching approximately $9500\,\mathrm{J/(s \cdot m^2{\cdot}K)}$, with adiabatic wall temperatures near 2740 K along the converging section. Transient thermal simulations conducted in ANSYS confirmed that the aluminum casing would exceed safe operating temperatures well within the 90-second burn envelope. To address this, an alternate design incorporating a thickened graphite insert was evaluated as a combined heat sink and insulator between the exhaust gases and the aluminum casing. While simulations of this configuration showed the aluminum remaining within acceptable thermal limits — with outer casing temperatures reaching approximately 391°C at 90 s — the increased graphite wall thickness added significant mass and manufacturing cost, straining the lander's mass budget. As a result, ablative nozzle materials are being actively considered as a lower-mass alternative capable of tolerating the thermal environment without relying on a thick structural heat sink.

Acknowledgments

The authors acknowledge the Georgia Institute of Technology for its institutional support and facilities, including the Montgomery Machining Mall within the Woodruff School of Mechanical Engineering. This work reflects the collective efforts of Propulsive Landers at Georgia Tech (GTPL), and the authors thank all members across operations, propulsion, avionics, structures, and guidance, navigation, and control for their dedication to advancing student-led reusable rocketry.

References

[1] Waxman, B., Zimmerman, J., Cantwell, B., Zilliac, G., and Wells, E., "Mass Flow Rate and Isolation Characteristics of Injectors for Use with Self-Pressurizing Oxidizers in Hybrid Rockets," , ???? URL `https://ntrs.nasa.gov/api/citations/20190001326/downloads/20190001326.pdf`.

[2] Halchak, J., and Cannon, J., "Materials for Liquid Propulsion Systems," , ???? URL `https://ntrs.nasa.gov/api/citations/20160008869/downloads/20160008869.pdf`.

[3] Banica, M. C., and Menko, "Dynamical Chilldown Model of a Liquid Hydrogen Feed System," *Journal of Propulsion and Power*, Vol. 29, 2013, pp. 975–981. https://doi.org/10.2514/1.b34658.

[4] Chen, N., Liu, S., Zhou, X., and Zhang, H.-B., "Small Solid-Model Rocket Design and Soft Landing Trajectory Planning," *Journal of Spacecraft and Rockets*, Vol. 61, 2024, pp. 1667–1679. https://doi.org/10.2514/1.a35919.

[5] Wei, S.-S., Li, M.-C., Lai, A., Chou, T.-H., and Wu, J.-S., "A Review of Recent Developments in Hybrid Rocket Propulsion and Its Applications," *Aerospace*, Vol. 11, No. 9, 2024, p. 739. https://doi.org/10.3390/aerospace11090739, URL https://doi.org/10.3390/aerospace11090739.

[6] Whitmore, S. A., Peterson, Z. W., and Eilers, S. D., "Closed-Loop Precision Throttling of a Hybrid Rocket Motor,"

Journal of Propulsion and Power, Vol. 30, No. 2, 2014, pp. 325–336. https://doi.org/10.2514/1.B34924, URL https://doi.org/10.2514/1.B34924.

[7] Ahn, B., Kang, H., Lee, E., Yun, Y., and Kwon, S., "Design of Multiport Grain with Hydrogen Peroxide Hybrid Rocket," *Journal of Propulsion and Power*, Vol. 34, 2018, pp. 1189–1197. https://doi.org/10.2514/1.b36949.

[8] Bisin, R., Paravan, C., Alberti, S., and Galfetti, L., "A New Strategy for the Reinforcement of Paraffin-Based Fuels Based on Cellular Structures: The Armored Grain—Mechanical Characterization," *Acta Astronautica*, Vol. 176, 2020, pp. 494–509. https://doi.org/10.1016/j.actaastro.2020.07.003, URL https://doi.org/10.1016/j.actaastro.2020.07.003.

[9] Bisin, R., and Paravan, C., "A New Strategy for the Reinforcement of Paraffin-Based Fuels Based on Cellular Structures: The Armored Grain—Ballistic Characterization," *Acta Astronautica*, Vol. 206, 2023, pp. 284–298. https://doi.org/10.1016/j.actaastro.2023.02.027, URL https://doi.org/10.1016/j.actaastro.2023.02.027.

[10] Leverone, F. K., Brooks, M. J., Pitot de la Beaujardiere, J.-F. P., and Veale, K. L., "Performance Sensitivity Study on a Blowdown Nitrous Oxide Paraffin Wax Hybrid Sounding Rocket," *Acta Astronautica*, Vol. 160, 2019, pp. 230–239. https://doi.org/10.1016/j.actaastro.2019.04.043, URL https://doi.org/10.1016/j.actaastro.2019.04.043.

[11] Karabeyoglu, M. A., and Cantwell, B. J., "Combustion of Liquefying Hybrid Propellants: Part 2, Stability of Liquid Films," *Journal of Propulsion and Power*, Vol. 18, No. 3, 2002, pp. 621–630. https://doi.org/10.2514/2.5976, URL https://doi.org/10.2514/2.5976.

[12] Yadav, G. A. K. R., N., "Experimental evaluation of HTPB/paraffin fuel blends for hybrid rocket applications," *Aerospace*, 2019.

[13] Karabeyoglu, M. A., Zilliac, G., Cantwell, B. J., DeZilwa, S., and Castellucci, P., "Scale-Up Tests of High Regression Rate Paraffin-Based Hybrid Rocket Fuels," *Journal of Propulsion and Power*, Vol. 20, No. 6, 2004, pp. 1037–1045. https://doi.org/10.2514/1.3340, URL https://doi.org/10.2514/1.3340.

[14] Eilers, S. D., and Whitmore, S. A., "Correlation of Hybrid Rocket Propellant Regression Measurements with Enthalpy-Balance Model Predictions," *Journal of Spacecraft and Rockets*, Vol. 45, No. 5, 2008, pp. 1010–1020. https://doi.org/10.2514/1.33804, URL https://doi.org/10.2514/1.33804.

[15] Daynes, S., "Isotropic Cellular Structure Design Strategies Based on Triply Periodic Minimal Surfaces," *Additive Manufacturing*, Vol. 81, 2024, p. 103982. https://doi.org/10.1016/j.addma.2024.103982, URL https://doi.org/10.1016/j.addma.2024.103982.

[16] Gerbal, N., and Durand, G., "Formulation of a Mechanically Improved Paraffin Fuel," *Proceedings of the 5th European Conference for Aeronautics and Space Sciences (EUCASS)*, Munich, Germany, 2013.

[17] Palacz, T., "Nitrous Oxide Application for Low-Thrust and Low-Cost Liquid Rocket Engine," *Proceedings of the 9th European Conference for Aeronautics and Space Sciences (EUCASS)*, Milan, Italy, 2017. EUCASS Paper 17-522.

[18] Dionysatos, I., "Design and Testing of a 1kN Class Paraffin-Fieled Hybrid Rocket Engine," *AIAA*, 2023.

[19] Bouziane, M., Bertoldi, A. E. M., Milova, P., Hendrick, P., and Lefebvre, M., "Performance Comparison of Oxidizer Injectors in a 1-kN Paraffin-Fueled Hybrid Rocket Motor," *Aerospace Science and Technology*, Vol. 89, 2019, pp. 392–406. https://doi.org/10.1016/j.ast.2019.04.009, URL https://doi.org/10.1016/j.ast.2019.04.009.

[20] Vignesh, B., and Kumar, R., "Effect of Multi-Location Swirl Injection on the Performance of Hybrid Rocket Motor," *Acta Astronautica*, Vol. 176, 2020, pp. 111–123. https://doi.org/10.1016/j.actaastro.2020.06.029, URL https://doi.org/10.1016/j.actaastro.2020.06.029.

[21] Bouziane, M., Bertoldi, A., Hendrick, P., and Lefebvre, M., "Experimental Investigation of the Axial Oxidizer Injectors Geometry on a 1-kN Paraffin-Fueled Hybrid Rocket Motor," *FirePhysChem*, Vol. 1, No. 4, 2021, pp. 231–243. https://doi.org/10.1016/j.fpc.2021.11.012, URL https://doi.org/10.1016/j.fpc.2021.11.012.

[22] La Luna, S., Foletti, N., Magni, L., Zuin, D., and Maggi, F., "A Two-Phase Mass Flow Rate Model for Nitrous Oxide Based on Void Fraction," *Aerospace*, Vol. 9, No. 12, 2022, p. 828. https://doi.org/10.3390/aerospace9120828, URL https://doi.org/10.3390/aerospace9120828.

[23] Piscitelli, F., Saccone, G., Gianvito, A., Cosentino, G., and Mazzola, L., "Characterization and Manufacturing of a Paraffin Wax as Fuel for Hybrid Rockets," *Propulsion and Power Research*, Vol. 7, No. 3, 2018, pp. 218–230. https://doi.org/10.1016/j.jppr.2018.07.005, URL https://doi.org/10.1016/j.jppr.2018.07.005.

[24] Brown, G. O., "(PDF) The History of the Darcy-Weisbach Equation for Pipe Flow Resistance," , 10 2002. URL https://www.researchgate.net/publication/242138088_The_History_of_the_Darcy-Weisbach_Equation_for_Pipe_Flow_Resistance.

[25] Chen, J., Gao, Q., and Zhang, Q., "Measurement and calculation of minor loss coefficient of 90-degree pipe bend," Vol. 3006, ????, pp. 012046–012046. https://doi.org/10.1088/1742-6596/3006/1/012046.

[26] Peterson, Z. W., Eilers, S. D., and Whitmore, S. A., "Closed-Loop Thrust and Pressure Profile Throttling of a Nitrous Oxide HTPB Hybrid Rocket Motor," *48th AIAA/ASME/SAE/ASEE Joint Propulsion Conference and Exhibit*, Atlanta, Georgia, 2012. https://doi.org/10.2514/6.2012-4200, URL https://doi.org/10.2514/6.2012-4200.

[27] Karabeyoglu, M. A., Altman, D., and Cantwell, B. J., "Combustion of Liquefying Hybrid Propellants: Part 1, General Theory," *Journal of Propulsion and Power*, Vol. 18, No. 3, 2002, pp. 610–620. https://doi.org/10.2514/2.5975, URL https://doi.org/10.2514/2.5975.